Accreting magnetars: a new type of high-mass X-ray binaries?

P. Reig,[1,2]⋆ J. M. Torrejón[3] and P. Blay[4]

[1] *IESL, Foundation for Research and Technology-Hellas, GR-71110 Heraklion, Crete, Greece*
[2] *Institute of Theoretical & Computational Physics, University of Crete, PO Box 2208, GR-710 03 Heraklion, Crete, Greece*
[3] *Instituto de Física Aplicada a las Ciencias y las Tecnologías, Universidad de Alicante, E 03080 Alicante, Spain*
[4] *IPL, Universidad de Valencia, PO BOX 22085, 46071 Valencia, Spain*

ABSTRACT

The discovery of very slow pulsations ($P_{spin} = 5560$ s) has solved the long-standing question of the nature of the compact object in the high-mass X-ray binary 4U 2206+54 but has posed new ones. According to spin evolutionary models in close binary systems, such slow pulsations require a neutron star magnetic field strength larger than the quantum critical value of 4.4×10^{13} G, suggesting the presence of a magnetar. We present the first *XMM–Newton* observations of 4U 2206+54 and investigate its spin evolution. We find that the observed spin-down rate agrees with the magnetar scenario. We analyse Integral Spacecraft Gamma-Ray Imager (ISGRI)/*INTErnational Gamma-RAy Laboratory* (*INTEGRAL*) observations of 4U 2206+54 to search for the previously suggested cyclotron resonance scattering feature at ∼30 keV. We do not find a clear indication of the presence of the line, although certain spectra display shallow dips, not always at 30 keV. The association of these dips with a cyclotron line is very dubious because of its apparent transient nature. We also investigate the energy spectrum of 4U 2206+54 in the energy range 0.3–10 keV with unprecedented detail and report for the first time the detection of very weak 6.5 keV fluorescence iron lines. The photoelectric absorption is consistent with the interstellar value, indicating very small amount of local matter, which would explain the weakness of the florescence lines. The lack of matter locally to the source may be the consequence of the relatively large orbital separation of the two components of the binary. The wind would be too tenuous in the vicinity of the neutron star.

Key words: binaries close – stars: emission line, Be – stars: magnetars – stars: neutron – X-rays: binaries.

1 INTRODUCTION

The X-ray source 4U 2206+54 is a peculiar member of the high-mass X-ray binary systems (HMXBs). In this type of X-ray binaries, the normal stellar component is a massive star, usually an O or B star, while the X-ray emitting component is generally a neutron star. Mass transfer in HMXBs may occur via the strong stellar wind of the optical companion as in systems containing supergiant stars, the so-called supergiant X-ray binaries[1] (SGXBs) or via the disc-like envelope of photospheric material around the equator of main-sequence companions. In this latter case, the system is called a Be/X-ray binary (BeXB). Wind-fed systems are normally persistent X-ray sources with X-ray luminosities of the order of 10^{35}–10^{36} erg s^{-1}, while most BeXBs are transient sources with episodes of violent

eruption in X-rays that may reach 10^{38} erg s^{-1}. The optical/X-ray properties of 4U 2206+54 do not fit in any of these two categories of HMXBs.

It is classified as an HMXB because it contains a neutron star orbiting an O-type companion (Negueruela & Reig 2001). However, 4U 2206+54 does not belong to the supergiant subgroup because the optical companion is a main-sequence star (Blay et al. 2006). The absence of any obvious long-term trends in the evolution of the Hα line spectral parameters and the lack of any correlation between the Hα line equivalent width (EW) and infrared magnitudes and colours differ from what it is expected in a typical BeXB. Optical and infrared studies indicate that the optical companion in 4U 2206+54 is an O9.5V star located at a distance of 2.6 kpc (Blay et al. 2006) with a higher than normal He abundance. The X-ray emission is the result of accretion from an abnormally slow wind (Ribó et al. 2006).

For a long time, the nature of the compact companion was debated. Recently, Reig et al. (2009) discovered a 5560-s modulation in the X-ray light curve that was interpreted as the spin period of the

⋆ E-mail: pau@physics.uoc.gr
[1] Accretion via an accretion disc is believed to occur in only three SGXBs due to the Roche lobe overflow.

neutron star. The discovery of very slow pulsations has solved the controversy on the nature of the compact object in 4U 2206+54, but has prompted new questions. According to spin evolutionary models in close binary systems, such slow pulsations require magnetic field strengths of the order of $\gtrsim 10^{14}$ G, that is, they require the system to harbour a magnetar (Finger et al. 2010; Ikhsanov & Beskrovnaya 2010).

The magnetic field strength can be estimated considering the neutron star spin evolution. Finger et al. (2010) derived an average rate of the spin frequency change of $\dot{\nu} = (-1.7 \pm 0.3) \times 10^{-14}$ Hz s^{-1}. Based on the slow pulsation period and the spin-down rate, they show that the 5560-s pulsations in the X-ray flux of 4U 2206+54 can be explained 'provided the neutron star in this system is a magnetar whose surface field at the present epoch exceeds 10^{14} G'.

However, these results are at odds with the tentative detection of a cyclotron resonance scattering feature (CRSF). Although the statistical significance of this feature is only marginal in any single measurement, it has been reported by three different observatories: *RXTE* (Torrejón et al 2004), *BeppoSAX* (Masetti et al. 2004) and *INTEGRAL* (Blay et al. 2005; Wang 2009) at different epochs. However, no sign of this feature has been detected in other observations with the same instruments onboard *RXTE* (Reig et al. 2009) and *INTEGRAL* (Wang 2010). If real, the detection of a CRSF at ∼30 keV would imply a magnetic field strength ($B/10^{12}$ G $\approx E_{cycl}/11.6$ keV) of 3.3×10^{12} G, typical of accretion-powered pulsars.

In this work, we analyse the first *XMM–Newton* observations of 4U 2206+54. We confirm the existence of the 5560-s X-ray pulsations, derive a new value of the spin-down rate and perform a detailed spectral study of the soft emission with unprecedented sensitivity. We also analyse ISGRI/*INTEGRAL* observation to search for the presence of the cyclotron line.

2 OBSERVATIONS AND DATA ANALYSIS

2.1 *XMM–Newton* observations

4U 2206+54 was observed by *XMM–Newton* on 2011 February 6 during revolution 2044. The observation (ObsID 0650640101) started at 03:39 h UT and lasted for ∼75 ks. The observation details for the instruments onboard *XMM–Newton* are presented in Table 1. The *XMM–Newton* Observatory (Jansen et al. 2001) includes three 1500 cm^2 X-ray telescopes each with a European Photon Imaging Camera (EPIC) at the focus. Two of the EPIC imaging spectrometers use MOS CCDs (Turner et al. 2001) and one uses PN CCDs (Strüder et al. 2001). Reflection Grating Spectrometers (RGS; den Herder 2001) are located behind two of the telescopes while the 30-cm optical monitor (OM) instrument has its own optical/ultraviolet telescope (Mason et al. 2001). All instruments were in operation during the observation. Data were reduced using the *XMM–Newton* Science Analysis System (SAS version 11.0).

We first reprocessed observation data files (ODFs) to obtain calibrated and concatenated event lists. The EPIC-PN analysis was performed on this ODF event file. We restricted the useful PN events to those with a pattern in the range 0–4 (single and doubles) and complying with the more strict selection criterion FLAG = 0, which omits parts of the detector area like border pixels and columns with higher offset.

Although the observation were made in the 'partial window' mode, the brightness of the source was so high that the EPIC instruments were affected by pile-up. Because the PN camera has a faster read-out time, it is less affected by this effect. Consequently, we used PN data in our timing and broad-band spectral analysis. PN spectra and light curves were generated by excluding the core of the point spread function. The same extraction region was used for both light curves and energy spectra. We extracted events from an annulus region with inner and outer radii 10 and 60 arcsec, respectively. Background files were obtained from a circular source-free region with a radius 30 arcsec centred approximately at the same distance as the read-out node (RAWY) as the source region. To achieve the best energy resolution and minimize further the effect of pile-up the final PN spectrum was created from single events only. The SAS tasks *rmfgen* and *arfgen* were used to generate source-specific response matrix files and auxiliary response files for spectral analysis. We rebinned the EPIC-PN spectrum to oversample the full width at half-maximum of the energy resolution by a factor of 3, and to have a minimum of 25 counts per bin to allow the use of the χ^2 statistic.

The SAS task *rgsproc* was used to produce calibrated RGS event lists, spectra and response matrices. The individual spectra of the same spectral order obtained from each of the two RGS instruments were combined (*rgscombine*) to produce the final RGS spectrum.

2.2 *INTEGRAL* observations

INTEGRAL is an ESA space mission with contributions from NASA and Russia dedicated to the observation of the hard X-rays/soft gamma-ray Universe (Winkler et al. 2003). The two main instruments onboard *INTEGRAL* are IBIS (Imager on Board the *INTEGRAL* Spacecraft) which operates in the 15 keV–10 MeV energy range (Ubertini et al. 2003) and SPI (SPectrometer on INTEGRAL) which operates in the 20 keV–8 MeV energy range (Vedrenne et al. 2003). IBIS, in turn, is composed of two detector layers, ISGRI operational in the 15–1000 keV range and Pixellated CSi Telescope working in the 0.175–10 MeV range (Labanti et al. 2003; Lebrun et al. 2003). At lower energies, the payload of *INTEGRAL* consists of the Joint European X-ray monitor, sensitive to X-rays in the 3–35 keV band (Lund et al. 2003) and the optical monitor OMC that covers the visual range 5000–6000 Å (Mas-Hesse et al. 2003).

INTEGRAL observations normally consist of a series of pointings called science windows (SCWs), 2–4 ks each. Since the launch of *INTEGRAL* in 2002 October, 4U 2206+54 has repeatedly appeared in the field of view of its instruments. However, the number of observations with a significant detection of the source (those with a detection level above 7σ) is relatively small. We have analysed all publicly available ISGRI observations from the beginning of the mission up to revolution 966 (2010 September). We selected the SCWs where the source was within 10° from the centre of the pointing and the detection level was above 7σ. This selection resulted in 37 SCWs. For each SCW an ISGRI spectrum was obtained. These spectra were combined together to produce an average ISGRI spectrum. The Integral Science Data Centre software OSA (Offline Scientific Analysis) version 9.0 was used in the data processing.

Table 1. *XMM–Newton* observation log.

Instrument	Mode	Filter	Exposure (ks)
EPIC-PN	Large window	Medium	74.8
MOS1	Small window	Medium	72.4
MOS2	Small window	Medium	72.4
RGS	Standard	–	76.4
OM	Image	Grism1	71.7
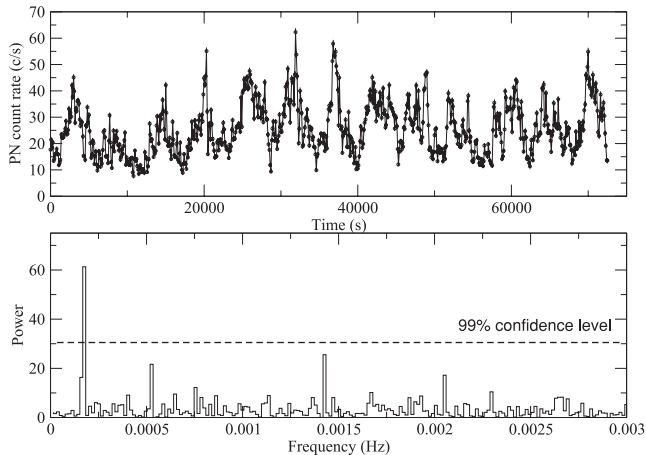
Figure 1. Upper panel: PN light curve 4U 2206+54. Time zero is MJD 555 98.17 and bin size is 100 s. Bottom panel: FFT using a 10-s binned light curve. A peak at ~0.17 mHz, representing the 5590-s pulsations, is clearly seen.

## 3 THE SPIN-PERIOD EVOLUTION

Prior to the determination of the spin period, we converted the arrival times to the Solar system barycentre. Then we generate a light curve in the 0.2–12 keV energy range with a bin size of 10 s. The last ~2300 s of the light curve were affected by high background. After removing this part the total duration of the light curve was 72.5 ks.

Fig. 1 shows the 0.2–12 keV PN light curve rebinned to 100-s bins and the fast Fourier transform (FFT) obtained from the 10-s binned light curve. A coherent periodicity is visible in the light curve and confirmed by the FFT. The maximum power is distributed around ~0.000 1775 Hz, corresponding to a period of ~5635 s. The power spectrum of 4U 2206+54 is characterized by strong red noise at low frequencies, which is well described by a power-law model with a slope of 1.5–1.7 (Reig et al. 2009). To assess the statistical significance of this peak and give a confidence detection limit (dashed line in Fig. 1), we first corrected for the presence of this type of noise by fitting a power-law function to the continuum. The power spectrum shown in Fig. 1 was created by multiplying the original power spectrum by 2 and dividing by the power-law model.

The small number of pulse cycles covered by the light curve (~13) prevented us from using the pulse phase connection technique (see e.g. Staubert, Klochkov & Wilms 2009 and references therein) to derive an accurate value of the spin period because the pulse profiles would not have sufficient statistics. Nevertheless, we can use other less accurate techniques to refine the value of the spin period. We used the CLEAN (Roberts, Lehár & Dreher 1987), Lomb–Scargle (Scargle 1982) and phase dispersion minimization (PDM; Stellingwerf 1978) algorithms. All these algorithms are implemented in the program PERIOD (version 5.0), distributed with the STARLINK Software Collection. Table 2 gives the results of the timing analysis. Another technique that achieves smaller errors is epoch folding (Leahy et al. 1983; Leahy 1987). We used the task *efsearch* of the XRONOS package and equation 6a in Leahy (1987) to estimate the error. We obtained $P_{spin} = 5591 \pm 3$ s. One more determination of the spin period was done with the software package PERIOD04 (Lenz & Breger 2005), which uses a discrete Fourier transform (DFT) algorithm and allows the estimation of uncertainties through Monte Carlo simulations. This method gave 5600 ± 5 s, where the error was estimated from the distribution of frequencies after running 1000 simulations. The mean spin period obtained as

Table 2. Spin-period determination.

| Method	P_{spin} (s)
CLEAN	5580 ± 107
Lomb–Scargle	5580 ± 107
PDM	5532 ± 105
DFT	5600 ± 5
Epoch folding	5591 ± 3
Mean	5586 ± 30
Weighted mean	5593 ± 3
Final adopted value	5593 ± 10
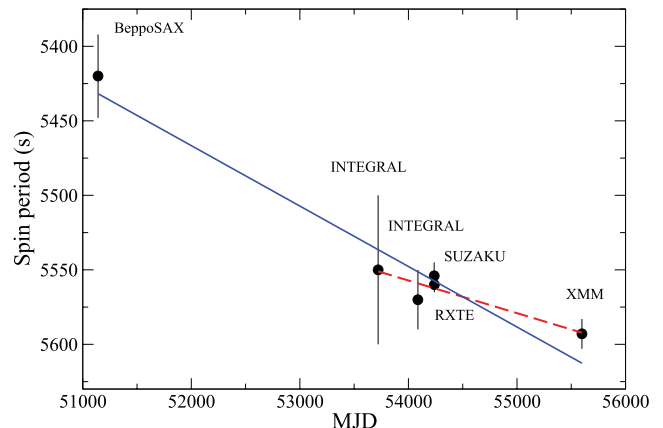
Figure 2. Spin-down evolution. The lines represent the best linear fit to all the data (solid line) and after removing the oldest data point (dashed line).

the average of the six methods is 5585 ± 30 s, where the error is the standard deviation of the measurements. A weighted mean gives 5593 ± 3 s. However, it should be noted that these calculations apply in the case that, in the absence of pulsations, the only noise present in the data is that due to counting statistics, i.e. white noise. Because 4U 2206+54 shows strong red noise in its power spectrum (Reig et al. 2009), Finger et al. (2010) used a more realistic approach and assumed that the natural log of the rates is (as opposed to just the rates) Gaussian distributed. Then they used the *Cash* statistics and compared it to the results obtained with the Lomb–Scargle method. They found that the pulse periods estimated from the peak of the Lomb–Scargle periodogram were shifted by 1–20 s (depending on the initial light curve) with respect to the maximum likelihood fit (minimization of the *Cash* statistic). Taking into account these statistical considerations, we adopted a final value of $P = 5593 \pm 10$ s.

Fig. 2 shows the spin-down evolution of 4U 2206+54. The data points come from Finger et al. (2010, *BeppoSAX* and *Suzaku*), Reig et al. (2009, *INTEGRAL* and *RXTE*) and Wang (2010, *INTEGRAL*). Using only the *BeppoSAX* and *Suzaku* measurements of the spin period, Finger et al. (2010) obtained a spin-down rate of $\dot{\nu} = (-1.7 \pm 0.3) \times 10^{-14}$ Hz s^{-1}. Fig. 2 shows that this trend continues up to present. A linear fit to all the data points gives $\dot{\nu} = (-1.5 \pm 0.2) \times 10^{-14}$ Hz s^{-1} with a correlation coefficient of 0.97 (solid line).

4 THE *XMM–NEWTON* SPECTRUM

The *XMM* observations allow us to investigate the low-energy part of the spectrum in 4U 2206+54 with unprecedented sensitivity.
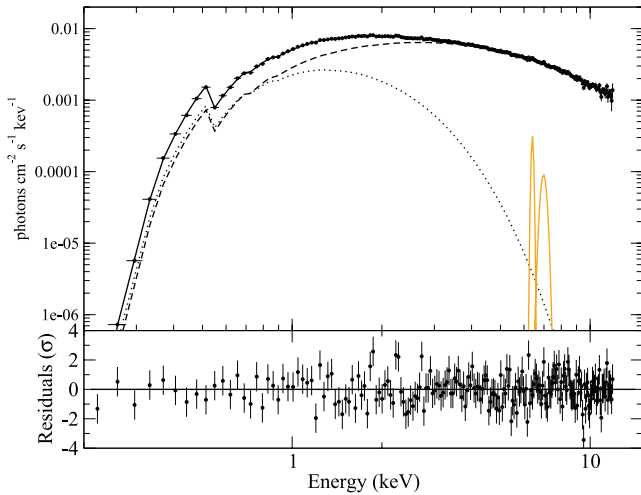
Figure 3. EPIC-PN energy spectrum. The BMC (dashed line) dominates the description of the continuum spectrum at high energies while a blackbody (dotted line) has been added to correct the excess at low energies.

Table 3. Best-fitting spectral parameters to the EPIC-PN spectrum. The luminosity and blackbody emitting radius were computed assuming a distance of 2.6 ± 0.3 kpc (Blay et al. 2006). Quoted errors are at 90 per cent confidence level for a single parameter. ABS: photoelectric absorption, BB: blackbody, BMC: bulk motion comptonization, PL: power law.

ABS*(BB+BMC)	
N_{H} ($\times 10^{21}$ cm^{-2})	2.23 ± 0.02
kT_{bb} (keV)	0.51 ± 0.02
R_{bb} (km)	1.3 ± 0.2
kT_{col} (keV)	$1.47^{+0.07}_{-0.04}$
α	$1.37^{+0.05}_{-0.4}$
L_{bb} ($\times 10^{35}$ erg s^{-1})	0.13
L_{BMC} ($\times 10^{35}$ erg s^{-1})	2.7
χ^2/dof	$0.98/197$
ABS*(BB+PL)	
N_{H} ($\times 10^{21}$ cm^{-2})	3.72 ± 0.08
kT_{bb} (keV)	1.63 ± 0.03
R_{bb} (km)	0.37 ± 0.04
Γ	0.94 ± 0.03
PL^a_{norm}	1.11 ± 0.04
L_{bb} ($\times 10^{35}$ erg s^{-1})	1.17
χ^2/dof	$1.25/200$
ABS*(BB+BB)	
N_{H} ($\times 10^{21}$ cm^{-2})	2.00 ± 0.05
kT_{bb1} (keV)	0.69 ± 0.02
R_{bb1} (km)	1.1 ± 0.1
kT_{bb2} (keV)	2.11 ± 0.02
R_{bb2} (km)	0.34 ± 0.04
χ^2/dof	$1.45/200$
$L_{0.3-2\,\mathrm{keV}}$ ($\times 10^{35}$ erg s^{-1})	0.16
$L_{2-10\,\mathrm{keV}}$ ($\times 10^{35}$ erg s^{-1})	2.21

$^a \times 10^{-2}$ ph keV^{-1} cm^{-2} s^1 at 1 keV.

4.1 The EPIC-PN spectrum

Fig. 3 shows the EPIC-PN spectrum of 4U 2206+54, covering the energy range 0.2–12 keV. This spectrum can be well represented by two-component models, affected by photoelectric absorption. The first component is a blackbody, which accounts for the softer part of the spectrum, while the second component dominates above ∼3 keV. Good fits to the EPIC spectral continuum are obtained when the second component is represented by a power law, by bulk motion Comptonization (BMC; Shrader & Titarchuk 1998) or even by another blackbody. The best-fitting parameters of these two combination of models are presented in Table 3.

The fit with the reduced χ^2 closest to 1 is obtained with the combination that includes the BMC. In this model, the power-law spectral index α yields a value larger than 1 which means that the Comptonization efficiency is high. Consequently, the illumination factor f, defined as the number of photons multiply scattered with respect to the number of injected photons by the thermal component, is $\gg 1$, that is to say, the spectrum appears completely Comptonized. The size of the seed soft photons production site can be estimated from the luminosity of the soft photons source $L_0 = \frac{L}{\ln(1/x_0)}$, where L is the resulting Comptonized luminosity and $x_0 = 2.8kT_{\mathrm{col}}/kT_e$ (Titarchuk, Mastichiadis & Kylafis 1997). Using the values in Table 3 and assuming a Comptonizing cloud of $kT_e \sim 50$ keV (as obtained in previous works, e.g. Torrejón et al 2004), we obtain $L_0 = 1.1 \times 10^{35}$ ergs s^{-1}. If the soft photon source is radiating like a blackbody of area πR_{W}^2, then we have

$$R_{\mathrm{W}} = 0.6\sqrt{L_0^{34}}(kT_{\mathrm{col}}/1\,\mathrm{keV})^{-2} \ [\mathrm{km}],$$

which yields $R_{\mathrm{W}} \approx 1$ km. This is consistent with the size of a hotspot over the neutron star surface. On the other hand, if we do not assume any temperature for the Comptonizing cloud and use instead the total luminosity for the BMC component, the resulting radius is 1.6 km, still very small and compatible with a hotspot.

Alternatively, the size of the emitting region can be estimated from the blackbody component. The luminosity of the soft excess turns out to be $L_{\mathrm{bb}} = 1.3 \times 10^{34}$ ergs s^{-1} which, for the temperature

given in Table 3, yields a circular radius[2] of $R_{\mathrm{bb}} \approx 2.4$ km. This is again too small to be produced by any material surrounding the neutron star. This would be consistent with a reprocessing region (ring) surrounding the hotspot, the accretion mound or the top of the shock front at the impact point and excludes the innermost parts of a hypothetical accretion disk.

Given the limited bandpass of *XMM*-EPIC cameras, one might be worried about what fraction of the spectrum is being really accounted for by Comptonization. As can be seen in Fig. 3, the BMC component is fitting the high-energy part of the spectrum while the blackbody is contributing, mainly, at energies below 3 keV. Nonetheless, it is perhaps convenient to give the fitting in terms of a phenomenological model composed of the addition of a power law and a blackbody modified at low energies by photoelectric absorption. These parameters are given in the middle part of Table 3.

[2] If the interpretation that the blackbody component represents emission from hotspots is correct, then it seems more natural to assume a circular area as the emitting region. However, the values found in the literature normally assume a spherical emitting region. For this reason, the radii in Table 3 correspond to a spherical emitting area. Note that if the soft photon source is taken to radiate as a blackbody *spherical* surface (i.e. $4\pi R_{\mathrm{W}}^2$), the corresponding radius would be *half* that obtained from a circular region.

As can be seen, the fit is acceptable, albeit with a higher value of the reduced χ^2. The most noticeable change is the increase in temperature of the blackbody component which is now contributing at higher energies (peak at 4 keV). The radius of the soft photon source would be $R_{bb} \simeq 0.7$ km (0.37 km if a spherical emitting region is considered), smaller than, but of the order of, that found under the Comptonization interpretation.

The radii obtained from the two-blackbody model are also consistent with emission from the polar caps (Table 3), although in this case the model shows the largest residuals.

The error in R_{bb} was obtained by propagating the errors from the best-fitting blackbody normalization N ($R_{bb} = \sqrt{N}D_{10}$) as given by the χ^2 fit and the error on the distance, which was estimated to be 0.3 kpc (Blay et al. 2006). D_{10} is the distance to the source normalized to 10 kpc.

A high signal-to-noise spectrum at low energies is also particularly interesting because it allows the determination of the hydrogen column density, N_H. The energy range 0.1–2.0 keV is the most suitable band for the derivation of N_H since cold gas mainly absorbs X-ray photons with energies lower than 2–3 keV. We find $N_H = (0.36 \pm 0.01) \times 10^{22}$, which is the most accurate determination of the absorption to the source measured so far. The N_H allows us to derive the optical extinction to the system. Using the calibration by Güver & Özel (2009), we obtain $A_V = 1.63 \pm 0.08$ mag or, assuming a standard reddening law, $E(B - V) = A_V/3.1 = 0.53$ mag, in excellent agreement with the value of 0.54 ± 0.05 mag derived from optical observations (Blay et al. 2006). This value agrees very well with the reddening derived using diffuse interstellar bands; hence, it is consistent with Galactic absorption along the line of sight to 4U 2206+54. We conclude that there is very little matter locally.

4.2 RGS spectrum

The low value of the reddening is further supported by the analysis of the RGS data. In Fig. 4, we show the RGS spectrum of the source in the wavelength range 6–20 Å (= 0.6–2 keV). The data from RGS 1 and 2 have been added and the resulting spectrum re-binned so that each bin has a minimum signal-to-noise ratio of 7. In order to detect the presence of any possible lines, the modelling of the underlying continuum is critical. Therefore, we take advantage of the broader energy range of PN and use the parameters deduced in the previous section as input.
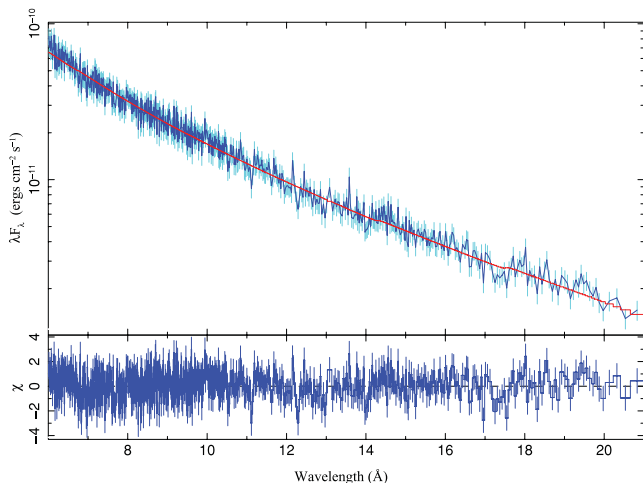

Figure 4. RGS spectrum.

Table 4. RGS model parameters.

Parameter	ABS*(BB)	ABS*(BB+PO)
$N_H (\times 10^{22}$ cm^{-2})	0.10 ± 0.02	0.16 ± 0.04
kT_{bb} (keV)	2.10 ± 0.30	1.95 ± 0.03
Norm$_{bb}$	0.0098 ± 0.0027	0.0082 ± 0.0004
χ^2_ν (dof)	1.19 (702)	1.19 (701)

Power-law photon index fixed at $\Gamma = 0.97$.

In this wavelength range the main contributor is the blackbody. Consequently, we tried a single absorbed blackbody as well as an absorbed power law plus blackbody. In the latter case, the power-law parameters were frozen while those of the blackbody were let to vary freely. The best-fitting parameters are given in Table 4. Two important conclusions can be drawn from this analysis. First, no emission lines from an ionized plasma are detected. This is in agreement with the PN analysis where the emission line candidates from photoionized species, if present, are extremely weak (see Section 4.3). Secondly, within the RGS interval the main indicators of the photoelectric absorption are the Ne edge at 14.2 Å and the Fe L edge at 17.5 Å. As can be seen, the edges are extremely shallow. This supports the low value of the photoelectric absorption obtained from the analysis of PN data.

4.3 Detection of emission lines

The X-ray spectrum of 4U2206+54 seems to be devoid of any strong emission features. The high sensitivity of *XMM*, however, allowed us to detect, for the first time, weak emission lines. The residuals are clearly structured around the Fe complex region at 6.5 keV and also around 2 keV. The region around 6.5 keV is shown in Fig. 5. These features can be fitted with two Gaussians centred at 6.46 ± 0.05 and at 6.99 ± 0.02 keV, respectively. Both lines show a width of $\sigma = 0.14$ keV but only in the first case the errors could be constrained (± 0.06) while we fixed the width for the second one. The lines are significant at 3σ. When the Gaussians are added, the χ^2 of the fit decreases from 251 for 202 degrees of freedom to
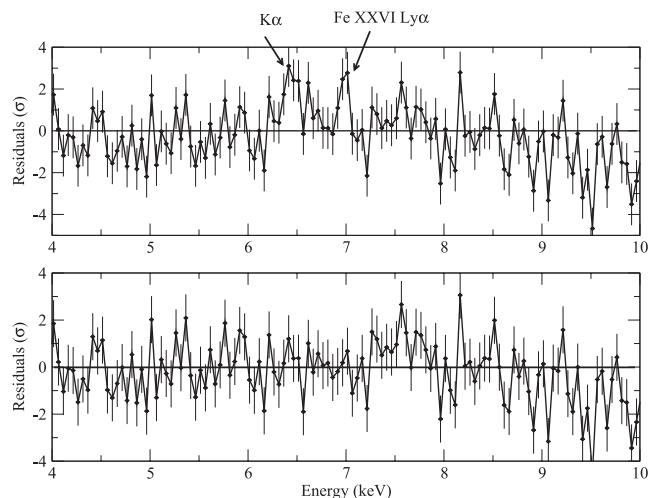

Figure 5. Residuals in number of sigmas of the fit to the EPIC-PN energy spectrum around the iron complex region. The lower and upper panels show the residuals with and without the inclusion of two Gaussian profiles, respectively.

Table 5. Emission line parameters.

Line	E	σ	Flux $(\times 10^{-5})$	EW
	(keV)	(keV)	(ph s^{-1} cm^{-2})	(eV)
Fe Kα	6.46 ± 0.05	0.14 ± 0.06	8.9 ± 3.0	25.0 ± 8.4
Fe XXVI Lyα	6.99 ± 0.02	0.14	5.2 ± 2.0	16.5 ± 13.2
Si XIV Lyα	2.22 ± 0.05	0.05	6.4 ± 2.0	7.4 ± 2.5

Numbers without errors were fixed at the quoted values.

214 for 198 degrees of freedom. The energy of these components is consistent with the Fe Kα (6.4 keV) transition from neutral Fe and the Fe XXVI Lyα (6.96 keV) transition from ionized H-like Fe. The parameters of these lines are shown in Table 5. As can be seen, even though the detection is firm, the EW is very small (25 and 16.5 eV, respectively). Consistently with the extreme weakness of the Fe Kα line, no Fe edge at 7.14 keV is detected.

The residuals around the 2 keV region can be fitted with a narrow Gaussian at 2.22 ± 0.05 keV. The centroid energy is consistent with the Si XIV Lyα transition of H-like Si. The line appears very narrow and cannot be resolved by the instrument. We fixed the width to 0.05 keV. The significance of this line is, however, low (2σ).

5 THE ISGRI SPECTRUM

Previous works (Masetti et al. 2004; Torrejón et al 2004; Blay et al. 2005; Wang 2009) have reported the possible presence of a CRSF at around 30 keV. All the detections of this feature were tentative because the statistical significance of any individual detection was $\lesssim 2\sigma$. Since the gamma-ray imager onboard *INTEGRAL* is sensitive to X-rays in the range 15–1000 keV and has been in operation for nearly 12 yr, it is a promising instrument to search for the cyclotron line. We obtained an ISGRI spectrum for each of the SCWs for which the source appeared with a detection level above 7σ and lay within $10°$ of the centre of the pointing. An average spectrum was created from the 37 resulting spectra. The average spectrum obtained from the 37 SCWs does not show any significant feature at the energy of the previous reported line. A single power-law component gives an acceptable fit ($\chi^2 = 28$ for 21 degrees of freedom) in the range 20–180 keV. The best-fitting photon index is 2.65 ± 0.08.

Fig. 6 shows the combined EPIC-PN and ISGRI spectra. The blackbody plus BMC and two-narrow-Gaussian model gives a very good fit (reduced $\chi^2 \approx 1$). The best-fitting values of the spectral parameters obtained from the fit of this model to the joined EPIC–ISGRI spectrum are consistent with those in Table 3, within errors. The energy spectral index is slightly larger, 1.7, compared to 1.5 of the EPIC-PN spectrum.

6 DISCUSSION

4U 2206+54 is a persistent X-ray source with relatively low luminosity ($L_X \lesssim 10^{36}$) compared to other accreting X-ray pulsars. It shows X-ray variability on time-scales of a few days with an amplitude of ~ 5 (Reig et al. 2009) and on time-scales of years by a factor of $\lesssim 100$ (Ribó et al. 2006). The short-term variability has most likely an orbital origin (a varying mass accretion rate due to its elliptical orbit, $e = 0.4$), while the long-term variability is probably due to oscillations in the wind density from the donor star (Ribó et al. 2006).
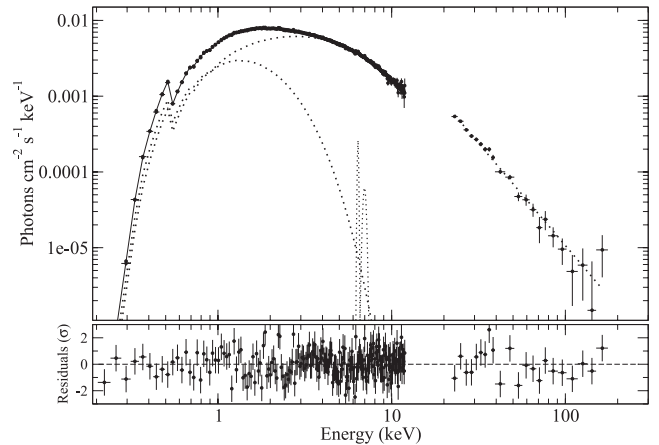
Figure 6. Joined EPIC-PN and ISGRI spectra. The dotted lines correspond to the blackbody plus bulk Comptonization model of Table 3.

Considerable progress has been made on the nature of this enigmatic system in the past years. The optical companion is an O9.5Vp, where p indicates that it is a peculiar star. The peculiarity of 4U 2206+54 is that the helium lines observed in the optical spectra (Blay et al. 2006) and stellar wind velocity (Ribó et al. 2006) are stronger and slower, respectively, than what is expected for a normal main-sequence O9.5 star. The highly debated issue of the nature of the compact companion, whether it is a neutron star or black hole, has been definitively solved in favour of the former with the discovery of X-ray pulsations (Reig et al. 2009).

4U 2206+54 has never been observed by any high-sensitivity instrument below 2 keV (*BeppoSAX* and *Suzaku* have ~ 10 times less effective area at ~ 0.3 and 1.5 keV, respectively, than *XMM–Newton*). Thus, the *XMM–Newton* observations represent an excellent opportunity to investigate the emission properties of 4U 2206+54 in the soft X-ray band.

6.1 The source environment

Fluorescent iron line emission provides strong evidence for the presence of material in the vicinity of the X-ray source. All previous observations of 4U 2206+54 failed to detect any iron line at or near 6.4 keV (Negueruela & Reig 2001; Masetti et al. 2004; Torrejón et al 2004; Reig et al. 2009). Upper limits for narrow (0.1 keV) and broad (0.5 keV) lines had been set in <56 and <65 eV, respectively (Masetti et al. 2004). These results imply that there is not much material intrinsic to the system. The agreement between the colour excess $E(B - V)$ derived from optical observations (Blay et al. 2005) and that obtained from our *XMM–Newton* observations (Section 4.1) would support this result.

In a recent survey of HMXB with *Chandra*, Torrejón et al. (2010) showed that the fluorescence Fe Kα line is present in virtually 100 per cent of the wind-fed HMXBs studied. The curve of growth shows that the reprocessing material is a spherical shell of near neutral Fe, formed in the stellar wind. It is surprising that although 4U 2206+54 is a wind-fed system this line has never been observed. The higher spectral resolution and sensitivity of *XMM–Newton* below 10 keV compared to previous missions allowed us to report the first detection of emission features at 6.4 and 7.0 keV. These features can be interpreted as Fe Kα and Fe XXVI Lyα from photoionized plasma, respectively.

Although statistically significant, these lines are weak. Somehow the compact object is not illuminating the stellar wind, as in the typical supergiant systems, even though the accretion process is taking place, efficiently. The source shows random variations in the light curve typical of wind accretors, as expected for an HMXB. Our results confirm that the X-ray source, however, is not deeply embedded into the stellar wind of the mass donor, yet it is continuously accreting. The large orbital separation would imply that the wind is too tenuous when it reaches the magnetosphere but the fraction of the stellar-wind mass-loss rate captured by the neutron star would still be large enough to power the X-rays. This fraction is (see e.g. Bozzo, Falanga & Stella 2008)

$$\dot{M}_{capt}/\dot{M}_w \simeq R_{acc}^2/(4a^2),$$

where a is the orbital separation and R_{acc} the accretion radius, which is the distance at which the inflowing matter is gravitationally focused towards the neutron star. It is given by

$$R_{acc} = 2GM/v_w^2 = 3.7 \times 10^{12} \, v_7^{-2} \,\,\text{cm}.$$

The stellar wind in 4U 2206+54 is abnormally slow with $v = 3.5 \times 10^7 \,\text{cm s}^{-1}$ (Ribó et al. 2006). Thus, the accretion radius in 4U 2206+54 is $R_{acc} = 3 \times 10^{11}$ cm.

The orbital period of 4U 2206+54 is still not known. Two modulations in the long-term X-ray light curve at 9.6 and 19.2 d have been attributed to the orbital period (Corbet, Markwardt & Tueller 2007). In either case, the neutron star is orbiting at a very large distance from the donor ($\sim 7R_*$ if $P_{orb} = 9.7$ d and $\sim 10R_*$ if $P_{orb} = 19$ d). Assuming the radius of 4U 2206+54 to be $R_* = 7.3\,R_\odot$ (Ribó et al. 2006), the orbital separation would result in $a = 3.6 \times 10^{12}$ and 5.3×10^{12} cm for the short- and long-orbital-period solutions, respectively.

Thus, the fraction of captured material would be $\dot{M}_{capt}/\dot{M}_w \simeq 0.002$ and 0.001, respectively. The mass-loss rate of an O9.5V star is $\sim 3 \times 10^{-8}\,\text{M}_\odot\,\text{yr}^{-1}$ (Ribó et al. 2006). Thus, $\dot{M}_{capt} \simeq 3 \times 10^{-11}\,\text{M}_\odot\,\text{yr}^{-1}$ or $2 \times 10^{15}\,\text{g s}^{-1}$, which is enough to power a luminosity of $\sim L_X \approx GM_{NS}\dot{M}_{capt}/R_{NS} \approx 3 \times 10^{35}\,\text{erg s}^{-1}$, as observed.

6.2 The X-ray spectrum

In order to investigate the nature of 4U 2206+54, it is illustrative to compare its X-ray spectrum with that of other types of strongly magnetized neutron-star systems: accreting X-ray pulsars and anomalous X-ray pulsars (AXPs). The former contain neutron stars with magnetic fields $B \sim 10^{12}$–10^{13} G, while AXPs are thought to harbour magnetars with $B \sim 10^{13}$–10^{15} G.

The spectra of many accreting X-ray pulsars show excess emission below ~ 2 keV. When this soft excess is modelled with a blackbody component, the temperature and emission radius strongly depend on the source luminosity (Hickox, Narayan & Kallman 2004). In BeXBs at low luminosity ($L_X \lesssim 10^{35}\,\text{erg s}^{-1}$), this soft component is believed to represent emission from the polar caps. The main piece of evidence supporting this interpretation is the size and temperature of the emitting area. The radius of the emitting region is typically $\lesssim 0.5$ km (Mukherjee & Paul 2005; La Palombara & Mereghetti 2006, 2007; La Palombara et al. 2009), significantly smaller than the assumed canonical size of the neutron star (~ 10 km). Thus, isotropic emission from the surface of the neutron star is ruled out. The blackbody temperature is $\gtrsim 1$ keV.

The X-ray spectra of AXPs in the 0.5–10 keV band are very soft and can best be described by a blackbody ($kT \sim 0.5$ keV) plus a very steep power-law model with $\Gamma \sim 3$–4 (Woods & Thompson 2006;

Kaspi 2007) or by two blackbody components with characteristic temperatures $\lesssim 1$ keV (Halpern & Gotthelf 2005).

The hard X-ray spectra (above 20 keV) of AXPs are characterized by a hard power-law tail extending up to 150 keV without any sign of turnover. The power-law photon index range $\Gamma \sim 1$–2, that is, much harder than the power laws seen below 10 keV (Götz et al. 2006). The X-ray spectrum of accreting X-ray pulsars above 20 keV also exhibits power-law tails. However, these are significantly softer ($\Gamma \sim 2$–3) than those of AXPs. Also, many accreting pulsars show exponential cutoffs at 30–50 keV (Blay et al. 2010).

The spectrum of 4U 2206+54 shows a soft excess at low energies. Irrespective of the model used, we find that the size of the emitting area in 4U 2206+54 is incompatible with the presence of an accretion disc and fits in the polar cap scenario. The temperature $kT_{bb} = 1.63$ keV and radius $R_{bb} = 370$ m of the blackbody component (Table 3) and the photon index ($\Gamma = 0.94$) are comparable to those seen in other low-luminosity accreting pulsars (La Palombara et al. 2009; Reig et al. 2009, and references therein). However, unlike most accreting X-ray pulsars, but similarly to AXPs, the hard power-law tail in 4U 2206+54 does not show any evidence for a cutoff below ~ 150 keV (Fig. 6). The hard spectrum in 4U 2206+54 is not as hard as in AXPs, though.

6.3 Is 4U 2206+54 a magnetar?

4U 2206+54 has been observed by many space observatories. A CRSF at ~ 30 keV has been reported in observations by *RXTE* (Torrejón et al 2004), *BeppoSAX* (Masetti et al. 2004) and *INTEGRAL* (Blay et al. 2005). All these detections were marginal (at $\lesssim 2\sigma$). Wang (2009) analysed *INTEGRAL* data of 4U 2206+54 and reported a harmonic of this feature at ~ 60 keV, although with very low significance. The alleged CRSF was only detected during a high state ($L_X \approx 2 \times 10^{35}\,\text{erg s}^{-1}$) but not during a low state ($L_X \approx 4 \times 10^{34}\,\text{erg s}^{-1}$) in the data analysed by Wang (2009). However, just a few days after the high state where the detection of the harmonic was reported, 4U 2206+54 exhibited two short-lived hard flares with peak luminosity $L_X \approx 1.3 \times 10^{36}\,\text{erg s}^{-1}$ and no CRSF was observed (Wang 2010). Quoted values of the luminosity are for the 20–100 keV range and a distance of 2.6 kpc (Blay et al. 2006). Likewise, Reig et al. (2009) did not find any evidence for a cyclotron line in the *RXTE* observations that led to the discovery of the X-ray pulsations. The observations by Reig et al. (2009) are particularly constraining because they analysed more than 138 ks worth of data with instruments capable to detect a cyclotron line at 30 keV. The fact that this feature, if real, is transient argues against its interpretation as a CRSF.

On the other hand, the cyclotron line shape is a strong function of viewing angle (Araya-Góchez & Harding 2000). Because of the long pulse period of 4U 2206+54, it might be possible that the cyclotron line in 4U 2206+54 is enhanced at certain pulse phases and suppressed at others. When analysing a pulse-phase *averaged* spectrum, the significance of the detection would depend on how many spectra at the right pulse phase are used. We explored this idea by performing pulse-phase *resolved* spectroscopy on the 2001 *RXTE* observations analysed in Torrejón et al (2004) and on ISGRI data taken on revolution 383 (2005 December) and revolution 510 (2006 December), but we did not find any significant change with pulse phase. This kind of analysis is hampered by low statistics.

An independent estimate of the magnetic field strength can be obtained considering the evolutionary track of the neutron star's spin period. Finger et al. (2010) derived an average rate of the spin frequency change between a *BeppoSAX* (1998 November) and a

Suzaku (2007 May) observation of $\dot{\nu} = (-1.7 \pm 0.3) \times 10^{-14}$ Hz s^{-1}, indicating that the rotation of the neutron star is slowing down. Based on the slow pulsation period and the spin-down rate, they show using a magneto-rotation model for the evolution of neutron stars, that the 5500-s pulsations in the X-ray flux of 4U 2206+54 can be explained provided the neutron star in this system is a magnetar whose surface field at the present epoch exceeds 10^{14} G. Indeed, the spin-down rate is related to the magnetic moment of the neutron star by (see e.g Ikhsanov & Beskrovnaya 2010)

$$\mu_m \approx 10^{32} k_t^{-1/2} (M_{1.5})^{1/2} I_{45}^{1/2} \dot{\nu}_{-14}^{1/2} P_{5500} \quad \text{G cm}^3,$$

where $I_{45} = I/10^{45}$ g cm^2 is the star's moment of inertia, k_t is a dimensionless parameter that accounts for the geometry of the accretion flux and it is close to 1 for spherical accretion, $\dot{\nu}_{-14} = \dot{\nu}/10^{-14}$ Hz s^{-1} is the rate at which the neutron star rotation changes with time and M is the mass of the neutron star in units of 1.5 M$_\odot$. From a detailed analysis of the magneto-rotational evolution of the neutron star in 4U 2206+54, Ikhsanov & Beskrovnaya (2010) concluded that its surface magnetic field may range from 5×10^{13} to 3×10^{15} G, depending on the geometry of the accretion flux outside the magnetosphere, with a most probable value in the interval $6-9 \times 10^{13}$ G. This scenario also requires that accretion in 4U 2206+54 must occur without the formation of an accretion disc. If an accretion disc were present, then the observed evolution of the rotation period in 4U 2206+54 would imply a magnetic field strength larger than 3×10^{15} G, which is rather difficult to account for with current models (Ikhsanov & Beskrovnaya 2010). The difficulty to accommodate an accretion disc was already mentioned by Torrejón et al (2004).

The estimate of the magnetic field strength based on the spin-down rate given by Finger et al. (2010) was determined using only two observations. As the authors state, 'it is very unlikely that the spin-down rate obtained from the *BeppoSAX* and *Suzaku* observations is valid on the long term since the pulsar would reach zero frequency in 300 yr'. Surprisingly, the spin-down rate obtained using all publicly available measurements of the spin period and the new value from *XMM–Newton* agrees well with that reported by Finger et al. (2010). As can be seen in Fig. 2, the spin-down rate does not show evidence of a break-up. A linear fit to all the measurements of the spin period of 4U 2206+54 gives a spin-down rate of $\dot{\nu} = (-1.5 \pm 0.2) \times 10^{-14}$ Hz s^{-1} with a correlation coefficient of 0.97. This rate implies a magnetic field of the order of $B \sim 10^{14}$ G.

If the 1998 *BeppoSAX* data point, i.e. the oldest measurement, is removed from the fit, then the spin-down rate decreases to half the previous value, $\dot{\nu} = (-7.5 \pm 2.0) \times 10^{-15}$ Hz s^{-1}, which would indicate that the neutron star has started to rotate at a faster rate. Still, the magnetic field derived from that spin-down rate (see the equation above) would be more than an order of magnitude stronger than common values seen in accreting X-ray pulsars.

Recently, a new theory of quasi-spherical accretion in X-ray pulsars has been developed (Shakura et al. 2012), where the dipole field in a wind-fed neutron star is given by (see e.g. Popov & Turolla 2012)

$$B_{12} \sim 8.1 \dot{M}_{16}^{1/3} V_{300}^{-11/3} \left(\frac{P_{1000}}{P_{\text{orb},300}} \right)^{11/12},$$

where $\dot{M}_{16}$ is the mass accretion rate in units of 10^{16} g s^{-1}, V_{300} is the wind velocity in units of 300 km s^{-1}, P_{1000} is the spin period in units of 1000 s and $P_{\text{orb},300}$ is the orbital period in units of 300 d. Substituting the values measured for 4U 2206+54: $\dot{M}_{16} = 0.2$, $V_{300} = 1.17$, $P_{1000} = 5.5$ and $P_{\text{orb},300} = 0.064$, the resulting magnetic

field is $B \sim 1.6 \times 10^{14}$ G, in agreement with the magnetic field obtained from the spin-down rate.

For a dipole magnetic field of $\sim 10^{14}$ G, the electron cyclotron line would appear at $E > 500$ keV, where the photon statistics are not good enough. On the other hand, a proton cyclotron line would appear at $E \sim 0.5(B/10^{14}G) = 0.5$ keV. Although a line with this energy should be observable with *XMM–Newton* detectors, it is in a region affected by strong interstellar absorption. Furthermore, no significant lines have been detected in the persistent emission of magnetars (Mereghetti 2008).

The picture of 4U 2206+54 that emerges from the available data at various bands of the electromagnetic spectrum is that of an intriguing system: a highly magnetized ($B \sim 10^{14}$ G) neutron star accreting matter from the stellar wind of an O-type main-sequence star. Is 4U 2206+54 a magnetar? 4U 2206+54 does not fit in the traditional definition of magnetars, namely very strongly magnetized ($B \sim 10^{14}$–10^{15} G), isolated neutron stars powered by magnetic energy. First, the magnetic field in 4U 2206+54 is in the lower end and most likely below the canonical range of magnetic fields in magnetars. Secondly, it is part of a binary system. Thirdly, X-rays are powered by accretion and the contribution to the X-ray luminosity from dissipation of the magnetic field is expected to be two to three orders of magnitude lower.

The characteristics of 4U 2206+54 would be closer to, but not fully consistent with the definition of AXPs (Mereghetti et al. 2002): a spinning down pulsar, with a soft X-ray spectrum, apparently not powered by accretion from a companion star, and with a luminosity larger than the available rotational energy loss of a neutron star. As shown in Section 6.2, the X-ray spectrum of 4U 2206+54 differs from that of AXPs.

Alternatively, one can simply define a magnetar as a neutron star with a magnetic field strength larger than the quantum critical value $B_q = m^2 cV3/\hbar e = 4.4 \times 10^{13}$ G at which the energy between Landau levels of electrons equals their rest mass. In this case, 4U 2206+54 would contain a magnetar accreting matter from a luminous companion. A more appropriate name for 4U 2206+54 would then be *accreting magnetar* (Ikhsanov & Beskrovnaya 2010).

6.4 Accreting magnetars as a class of systems

The idea that wind-fed X-ray pulsars may contain a supercritical highly magnetized neutron star has been discussed in previous works. The SGXB 2S 0114+650 is the accreting X-ray pulsar with the longest period (2.7 h). No cyclotron line has been reported in this system. Li & van den Heuvel (1999) argue that, to interpret such a long spin period, the magnetic field strength of this pulsar must have been initially $\gtrsim 10^{14}$ G.

Bozzo et al. (2008) showed that the large luminosity swings between quiescence and outbursts (up to $\sim 10^5$) seen in supergiant fast X-ray transients (SFXT) can be explained as a result of transitions across different inhibition of accretion regimes. These regimes include inhibition due to the magnetic and centrifugal barriers. In either case, magnetar-like fields can be attained if the spin period of the system is long ($\gtrsim 1000$ s) or the system is luminous ($L_X \gtrsim 10^{36}$ erg s^{-1}).

Another candidate for accreting magnetar is the wind-fed SGXB GX 301-2. Doroshenko et al. (2010) showed that a very strong magnetic field ($2-3 \times 10^{14}$ G) is required to explain the long pulse period of this system. A cyclotron line at 30–45 keV, implying a magnetic field of the order of 5×10^{12} G (Kreykenbohm et al. 2004; La Barbera et al. 2005), has been observed in GX 301-2.

This magnetic field is well below the critical value. However, these contradicting results can be reconciled if the line-forming region is situated far above (2–$3\,R_{\mathrm{NS}}$) the neutron star's surface, i.e. in the accretion column (Doroshenko et al. 2010). Another system that might belong to the class of highly magnetized HMXB is IGR J16358$-$4726, although its nature is much less certain (Patel et al. 2007)

The main difference of 4U 2206+54 with respect to 2S 0114+650, GX 301-2 and SFXTs is that 4U 2206+54 contains a main-sequence star, and hence a still younger system than those with supergiant companions. 4U 2206+54 would be the natural progenitor of SGXBs (Ribó et al. 2006). However, 4U 2206+54 may not be the only non-supergiant system with a likely highly magnetized neutron star. The magnetic field of the BeXB X Per may also lie in the magnetar range if a slow accretion wind is assumed (Doroshenko et al. 2012).

By comparing the common properties of these systems, we can identify the following general characteristics of accreting magnetar binaries.

(1) They contain slowly rotating neutron stars ($P_{\mathrm{spin}} \gtrsim 500\,\mathrm{s}$) with magnetic fields above the quantum critical value ($4.4 \times 10^{13}\,\mathrm{G}$) but lower than a few times $10^{14}\,\mathrm{G}$.

(2) They are persistent X-ray sources with luminosities in the range 10^{35}–$10^{36}\,\mathrm{erg\,s^{-1}}$ with long-term amplitude of X-ray variability below two orders of magnitude.

(3) They are young systems ($\lesssim 10^6\,\mathrm{yr}$), undergoing spherical wind accretion from luminous companions (OB stars) with abnormally low stellar wind velocity ($\lesssim 400\,\mathrm{km\,s^{-1}}$).

(4) Although brief spin-up episodes may occur, spin-down dominates the longterm with relatively short spin-down time-scales $\tau \sim P/\dot{P} \lesssim 10^3\,\mathrm{yr}$.

7 CONCLUSION

With the discovery of X-ray pulsations, the highly debated issue of the nature of the compact companion has been solved, but have posed new questions. The combination of slow pulsations and long-term spin-down of the neutron star can be understood assuming that the magnetic field of the neutron star is of the order of $10^{14}\,\mathrm{G}$. We have obtained a new value of the spin-down rate and shown that it is consistent with a supercritical magnetic field. We searched for the presence of a cyclotron line in the hard X-ray spectrum of 4U 2206+54, but we did not find any significant feature at the previously reported energies. 4U 2206+54 adds up to a growing population of highly magnetized neutron stars in binary systems, with magnetic field strengths in the magnetar range, whose X-ray emission is powered by accretion.

ACKNOWLEDGMENTS

REFERENCES

Araya-Góchez R. A., Harding A. K., 2000, ApJ, 544, 1067
Blay P., Ribó M., Negueruela I., Torrejón J. M., Reig P., Camero A., Mirabel I. F., Reglero V., 2005, A&A, 438, 963

Blay P., Negueruela I., Reig P., Coe M. J., Corbet R. H. D., Fabregat J., Tarasov A. E., 2006, A&A, 446, 1095
Blay P., Martínez-Núñez S., Reig P., Connell P., Torrejón J. M., Reglero V., 2010, Proc. the 8th INTEGRAL Workshop: 'The Restless Gamma-ray Universe'. Dublin Castle, Dublin
Bozzo E., Falanga M., Stella L., 2008, ApJ, 683, 1031
Corbet R. H. D., Markwardt C. B., Tueller J., 2007, ApJ, 655, 458
den Herder J. W. et al., 2001, A&A, 365, L7
Doroshenko V., Santangelo A., Suleimanov V., Kreykenbohm I., Staubert R., Ferrigno C., Klochkov D., 2010, A&A, 515, A10
Doroshenko V., Santangelo A., Kreykenbohm I., Doroshenko R., 2012, A&A, 540, L1
Finger M. H., Ikhsanov N. R., Wilson-Hodge C. A., Patel S. K., 2010, ApJ, 709, 1249
Götz D., Mereghetti S., Tiengo A., Esposito P., 2006, A&A, 449, L31
Güver T., Öxel F., 2009, MNRAS, 400, 2050
Halpern J. P., Gotthelf E. V., 2005, ApJ, 618, 874
Hickox R. C., Narayan R., Kallman T. R., 2004, ApJ, 614, 896
Ikhsanov N. R., Beskrovnaya N. G., 2010, Astrophys., 53, 2
Jansen F. et al., 2001, A&A, 365, L1
Kaspi V. M., 2007, Ap&SS, 308, 1
Kreykenbohm I., Wilms J., Coburn W., Kuster M., Rothschild R. E., Heindl W. A., Kretschmar P., Staubert R., 2004, A&A, 427, 975
La Barbera A., Segreto A., Santangelo A., Kreykenbohm I., Orlandini M., 2005, A&A, 438, 617
La Palombara N., Mereghetti S., 2006, A&A, 455, 283
La Palombara N., Mereghetti S., 2007, A&A, 474, 137
La Palombara N., Sidoli L., Esposito P., Tiengo A., Mereghetti S., 2009, A&A, 505, 947
Labanti C. et al., 2003, A&A, 411, L149
Leahy D. A., 1987, A&A, 180, 275
Leahy D. A., Darbro W., Elsner R. F., Weisskopf M. C., Kahn S., Sutherland P. G., Grindlay J. E., 1983, ApJ, 266, 160
Lebrun F. et al., 2003, A&A, 411, L141
Lenz P., Breger M., 2005, Commun. Asteroseismol., 146, 53
Li X.-D., van den Heuvel E. P. J., 1999, ApJ, 513, L45
Lund N. et al., 2003, A&A, 411, L231
Mas-Hesse J. M. et al., 2003, A&A, 411, L261
Masetti N., Dal Fiume D., Amati L., Del Sordo S., Frontera F., Orlandini M., Palazzi E., 2004, A&A, 423, 311
Mason K. O. et al., 2001, A&A, 365, L36
Mereghetti S., 2008, A&AR, 15, 225
Mereghetti S., Chiarlone L., Israel G. L., Stella, S., 2002, in Becker W., Lesch H., Trümper J., eds, Proc. 270. WE-Heraeus Seminar on Neutron Stars, Pulsars, and Supernova Remnants. MPE Report 278. Max Planck Institute for Extraterrestrial Physics, Garching, p. 29
Mukherjee U., Paul B., 2005, A&A, 431, 667
Negueruela I., Reig P., 2001, A&A, 371, 1056
Patel S. K. et al., 2007, ApJ, 657, 994
Popov S. B., Turolla R., 2012, MNRAS, 421, L127
Reig P., Torrejón J. M., Negueruela I., Blay P., Ribó M., Wilms J., 2009, A&A, 494, 1073
Ribó M., Negueruela I., Blay P., Torrejón J. M., Reig P., 2006, A&A, 449, 687
Roberts D. H., Lehár J., Dreher J. W., 1987, AJ, 93, 968
Scargle J. D., 1982, ApJ, 263, 835
Shakura N., Postnov K., Kochetkova A., Hjalmarsdotter L., 2012, MNRAS, 420, 216
Shrader C., Titarchuk L., 1998, ApJ, 499, L31
Staubert R., Klochkov D., Wilms J., 2009, A&A, 500, 883
Stellingwerf R. F., 1978, ApJ, 224, 953
Strüder L. et al., 2001, A&A, 365, L18
Titarchuk L., Mastichiadis A., Kylafis N. D., 1997, ApJ, 487, 834
Torrejón J. M., Kreykenbohm I., Orr A., Titarchuk L., Negueruela I., 2004, A&A, 423, 301
Torrejón J. M., Schulz N. S., Nowak M. A., Kallman T. R., 2010, ApJ, 715, 947
Turner M. J. L. et al., 2001, A&A, 365, L27

Ubertini P. et al., 2003, A&A, 411, L131
Vedrenne G. et al., 2003, A&A, 411, L63
Wang W., 2009, MNRAS, 398, 1428
Wang W., 2010, A&A, 520, A22
Winkler C. et al., 2003, A&A, 411, L1

Woods P. M., Thompson C., 2006, in Lewin W., van der Klis M., eds, Compact Stellar X-ray Sources. Cambridge Astrophys. Seri., No. 39. Cambridge Univ. Press, Cambridge, p. 547

This paper has been typeset from a TEX/LATEX file prepared by the author.